
Mapping of Lymphatic Drainage from the Prostate Using Filtered ^{99m}Tc -Sulfur Nanocolloid and SPECT/CT

Youngho Seo¹⁻³, Carina Mari Aparici^{1,4}, Chien Peter Chen², Charles Hsu², Norbert Kased², Carole Schreck¹, Nick Costouros¹, Randall Hawkins^{1,3}, Katsuto Shinohara^{2,5}, and Mack Roach III^{2,5}

¹Department of Radiology and Biomedical Imaging, University of California, San Francisco, California; ²Department of Radiation Oncology, Helen Diller Family Comprehensive Center, University of California, San Francisco, California; ³Joint Graduate Group in Bioengineering, University of California, San Francisco and Berkeley, California; ⁴San Francisco Veterans Affairs Medical Center, San Francisco, California; and ⁵Department of Urology, University of California, San Francisco, California

We have developed a practice procedure for prostate lymphoscintigraphy using SPECT/CT and filtered ^{99m}Tc -sulfur nanocolloid, as an alternative to the proprietary product ^{99m}Tc -Nanocoll, which is not approved in the United States. **Methods:** Ten patients were enrolled for this study, and all received radiotracer prepared using a 100-nm membrane filter at a commercial radiopharmacy. Whole-body scans and SPECT/CT studies were performed within 1.5–3 h after the radiotracer had been administered directly into 6 locations of the prostate gland under transrectal ultrasound guidance. The radiation dose was estimated from the first 3 patients. Lymphatic drainage mapping was performed, and lymph nodes were identified. **Results:** The estimated radiation dose ranged from 3.9 to 5.2 mSv/MBq. The locations of lymph nodes draining the prostate gland were similar to those found using the proprietary product. **Conclusion:** When the proprietary radiolabeled nanocolloid indicated for lymphoscintigraphy is not available, prostate lymph node mapping and identification are still feasible using filtered ^{99m}Tc -sulfur nanocolloid.

Key Words: prostate cancer; sulfur colloid; SPECT/CT; lymphatic mapping; sentinel node

J Nucl Med 2011; 52:1068–1072

DOI: 10.2967/jnumed.110.085944

It is estimated that 50% or more patients with high-risk prostate cancer will experience a relapse after definitive treatment (1). There are substantial data suggesting that many of these relapses may be due to microscopic metastasis in the pelvic lymph nodes (2–4). Recent surgical data have indicated that the incidence of positive nodes is higher than once thought (2).

Nomogram predictors (5) help identify a potential high risk of involved pelvic nodes. To confirm the microscopically involved nodes, lymphadenectomy combined with

pathologic analysis is necessary. Radical prostatectomy combined with an extended pelvic lymph node dissection (6) is one of the standard treatments for localized prostate cancer. However, in some cases, this treatment represents an overly aggressive and invasive approach.

External-beam radiotherapy or brachytherapy is presented with the same challenges. However, there is no method to assess nodal involvement unless anatomic imaging shows enlarged (>1 cm in diameter) lymph nodes. Recent studies suggest therapeutic value to treating potentially involved nodes by radiation (1). For example, the phase III trial by the Radiation Therapy Oncology Group (RTOG-9413) demonstrated that prophylactic pelvic lymph node irradiation improves progression-free survival for high-risk patients, suggesting that treatment of the primary tumor and local lymph nodes can be curative (7).

Pelvic irradiation can increase the probability of treatment side effects. The exact volume of nodes to include in the radiation field is therefore critical and has been much debated (8). Currently, most whole-pelvis radiotherapy planning is based on assumptions about standardized anatomic lymphatic drainage patterns (9). However, as shown by the results of radioguided surgical lymph node dissection, the patterns of each patient's lymphatic drainage from the prostate are highly variable (9,10).

Whole-pelvis irradiation of patient-specific lymphatic drainage with a highly conformal radiotherapy technique such as intensity-modulated radiotherapy may improve long-term tumor control outcomes (11). ^{99m}Tc -nanocolloids (colloidal particles < 100 nm) can be used to achieve personalized whole-pelvis radiation planning (9,12).

The most popular ^{99m}Tc -nanocolloid is a commercial product called ^{99m}Tc -Nanocoll (GE Healthcare), a colloid of human serum albumin (13). Extensive studies using this nanocolloid have been performed to map the sentinel lymph nodes of the prostate (14–16). However, this product has not yet received clearance from the U.S. Food and Drug Administration. In the United States, ^{99m}Tc -sulfur colloid is used in breast lymphoscintigraphy as well as for other applications (17). The ^{99m}Tc -sulfur colloid can be formed into a nanocolloid through the use of a 100-nm polycarbon-

Received Dec. 9, 2010; revision accepted Feb. 28, 2011.

For correspondence or reprints contact: Youngho Seo, Department of Radiology and Biomedical Imaging, University of California, San Francisco, 185 Berry St., Ste. 350, San Francisco, CA 94107-1739.

E-mail: youngho.seo@ucsf.edu

COPYRIGHT © 2011 by the Society of Nuclear Medicine, Inc.

TABLE 1

Comparison of Absorbed Dose Estimates (mSv/MBq) for ^{99m}Tc-Nanocoll and Filtered ^{99m}Tc-Sulfur Nanocolloid

Region	Reference (^{99m} Tc-Nanocoll) (20)	Patient 1	Patient 2	Patient 3
Whole body	7.6	4.0	3.9	5.2
Bladder	11.3	12.8	13.8	21.1
Liver	26.3	10.6	10.9	8.1
Spleen	16.5	12.4	9.4	37.5
Marrow	22.1	5.8	4.2	4.0

ate membrane filter, resulting in a range of particle sizes similar to that of ^{99m}Tc-Nanocoll (13). The important factor contributing to the kinetic properties of a radiocolloid is the distribution of particle sizes, and that factor has yet to be studied for filtered ^{99m}Tc-sulfur nanocolloid for prostate lymphoscintigraphy. We report our feasibility study of a SPECT/CT practice procedure we developed for prostate lymphoscintigraphy using filtered ^{99m}Tc-sulfur nanocolloid.

MATERIALS AND METHODS

Subject Recruitment and Adverse Event Monitoring

Subjects were recruited following a protocol approved by the Institutional Review Board. The filtered ^{99m}Tc-sulfur nanocolloid,

as a Food and Drug Administration–approved agent, was used for this open-label indication of lymph node scintigraphy. To be included, patients had to have a definitive diagnosis of prostate cancer, be clinically eligible to receive intensity-modulated radiotherapy with pelvic lymph nodal irradiation, and be scheduled for such treatment. Ten patients (age range, 56–81 y; prostate-specific antigen level, 3.55–70 ng/mL) were enrolled. Reportable adverse events were to be communicated 1 wk after radiotracer administration, but no adverse events occurred.

Administration of Agent

An arrangement was made with a local commercial radiopharmacy (GE Healthcare) that all orders for this study were to be prepared using a 100-nm membrane filter. After ^{99m}Tc-sulfur colloid is passed through a 100-nm polycarbonate membrane filter, most colloidal particles (~90%) are between 30 and 80 nm, with a peak at 53.9 nm (18). The agent was administered in the Urology Clinic at the University of California, San Francisco, Medical Center by one urologist with transrectal ultrasound guidance.

Filtered ^{99m}Tc-sulfur nanocolloid (40.7–111 MBq) was divided equally into 6 fractions of 0.5 mL each and was administered into 3 locations (apex, mid portion, and base) for each lobe (left and right) of the prostate gland. Although the administration was supposed to be evenly distributed to all 6 locations, we noted that some patients received uneven doses resulting in uneven flow patterns of nodal uptake.

Whole-Body and SPECT/CT Parameters

Our studies used a SPECT/CT system with a low-amperage CT scanner (Infinia Hawkeye 4; GE Healthcare) at the University of

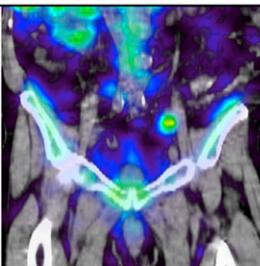
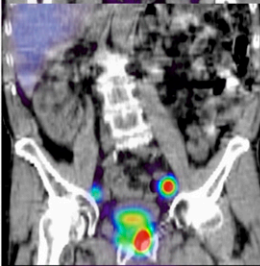
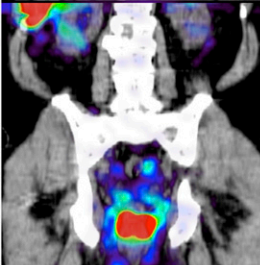
Patient	Age (y)	Injected dose (MBq)	Areas of lymph nodes identified	SPECT/CT
1	76	93	1) Bilateral external iliac 2) Bilateral common iliac 3) Low aortocaval region	
2	75	104	4) Bilateral external iliac (left > right) 5) Bilateral common iliac 6) Bilateral paraaortic (up to the level of the renal arteries)	
3	74	67	7) Bilateral external iliac (left > right) 8) Bilateral common iliac 9) Bilateral low paraaortic 10) Left paraaortic up to the level of the renal artery	

FIGURE 1. Age distribution, radiotracer administration, identified lymph node locations, and representative coronal view of SPECT/CT for study patients 1–3.

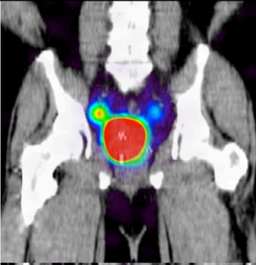
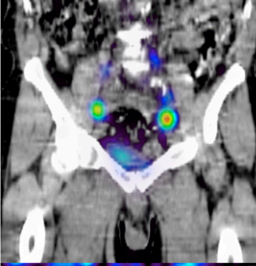
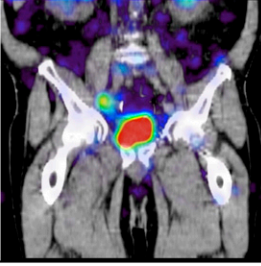
Patient	Age (y)	Injected dose (MBq)	Areas of lymph nodes identified	SPECT/CT
4	62	105	<ol style="list-style-type: none"> 1) Bilateral external iliac (right > left) 2) Bilateral common iliac 3) Bilateral paraaortic up to the level of the renal arteries 	
5	76	96	<ol style="list-style-type: none"> 4) Bilateral external iliac 5) Bilateral common iliac 6) Common iliac of the promontory 7) Subaortic common iliac 8) Bilateral paraaortic up to T12 level 9) Parapancreatic 	
6	78	41	<ol style="list-style-type: none"> 10) Bilateral external iliac 11) Bilateral internal iliac 12) Low bilateral paraaortic 	

FIGURE 2. Age distribution, radiotracer administration, identified lymph node locations, and representative coronal view of SPECT/CT for study patients 4–6.

California, San Francisco, China Basin Imaging Center. All SPECT images were reconstructed using ordered-subsets expectation maximization involving CT-based attenuation correction. The SPECT projections were acquired with a 128×128 matrix over 60 angles covering 360° at 15 s per stop. The reconstructed images were $64 \times 64 \times 64$ matrices postfiltered using a Butterworth filter. The anteroposterior whole-body scans were obtained before the SPECT/CT scans to ensure a sufficient distribution of filtered ^{99m}Tc -sulfur nanocolloid from the gland. SPECT/CT covering the pelvis and thorax was performed 1.5–3 h after administration. For the matching SPECT field of view, abdominopelvic CT was performed without a contrast agent. A tube voltage of 140 kVp and tube current of 2.5 mA were used, and the data were acquired using a 256×256 matrix and a 5-mm slice thickness. The filtered backprojection algorithm provided by the manufacturer was used for CT reconstruction.

Radiation Dose Estimation Using Simple Biokinetic Data

For the first 3 patients, we performed whole-body scans after SPECT/CT to obtain additional datasets for radiation dose estimates. For logistic convenience, we applied a simple biokinetic analysis based on 3 time points of radiotracer distribution. The first time point was not from imaging but was based on the assumption that initially the radiotracer is localized only to the administration site—the prostate gland. The 2 additional time points were before and after SPECT/CT.

OLINDA/EXM software (version 1.1) (19) was used to estimate radiation dose. We calculated residence times in the prostate, liver, and spleen from the whole-body scans using a conjugate-

view method and phantom measurements that corrected for image-pixel differences in radioactivity in anterior and posterior views. For phantom measurements, we used a 6-mL syringe with a clear acrylic attenuator of known activity, calibrated using a dose calibrator.

Lymph Node Identification and Drainage Mapping

The lymphoscintigraphy results were interpreted by attending nuclear medicine physicians and then again by one of the study investigators. We used SPECT/CT images for identifying lymph nodes and drainage patterns. The identification of sentinel lymph nodes and of all secondary nodes identifiable from the imaging studies was noted in the reports.

RESULTS

Radiation Dose Estimates

The reported radiation dose estimate for ^{99m}Tc -Nanocoll is an effective dose of 7.6 mSv/MBq (20). Data from the 3 patients showed an effective dose of 3.9–5.2 mSv/MBq for the filtered ^{99m}Tc -sulfur nanocolloid, slightly lower than the effective dose from ^{99m}Tc -Nanocoll (Table 1). Even with injected doses that were lower (40.7–111 MBq) than the typical dose of ^{99m}Tc -Nanocoll (200 MBq), we were able to visualize uptake in lymph nodes draining the injection site within 1.5–3 h after administration. From the radiation dose estimation data, we also found that hepatic clearance of filtered ^{99m}Tc -sulfur nanocolloid is slightly faster than that of ^{99m}Tc -Nanocoll.

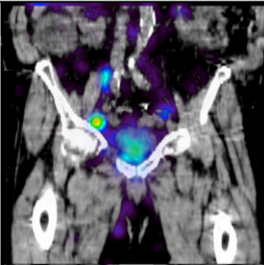
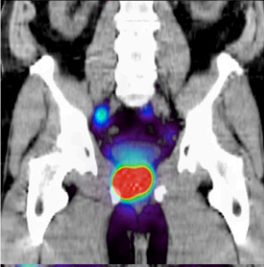
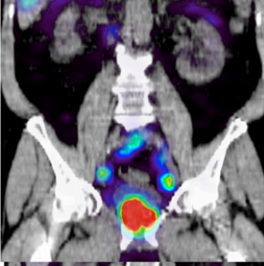

Patient	Age (y)	Injected dose (MBq)	Areas of lymph nodes identified	SPECT/CT
7	81	44	1) Bilateral inguinal 2) Bilateral external iliac 3) Right common iliac	
8	56	111	4) Bilateral external iliac 5) Bilateral common iliac 6) Common iliac of the promontory 7) Subaortic common iliac	
9	66	90	8) Left inguinal 9) Bilateral external iliac 10) Bilateral common iliac 11) Common iliac of the promontory 12) Subaortic common iliac 13) Bilateral paraaortic lymph nodes up to T12 level	
10	65	107	14) Bilateral external iliac (right > left) 15) Bilateral common iliac (right > left) 16) Low left paraaortic	

FIGURE 3. Age distribution, radiotracer administration, identified lymph node locations, and representative coronal view of SPECT/CT for study patients 7–10.

Lymph Node Identification

One criterion for the success of this procedure was to be able to image lymph node uptake outside the prostate within 1–3 h, and our results were consistent with that expectation.

Also as expected, lymph nodes were sometimes identified outside the pelvic area, a common feature of the prostatic lymphatic drainage pattern. Figures 1–3 show the demographics, injected dose, and lymphatic uptake locations for each patient. We also show a coronal SPECT/CT view displaying at least one lymph node that took up filtered ^{99m}Tc -sulfur nanocolloid. A descriptive list of lymph nodes identified as draining the prostate gland is also included in Figures 1–3.

DISCUSSION

In this report, we have shown that the nonproprietary filtered ^{99m}Tc -sulfur nanocolloid can be used to perform

prostate lymphoscintigraphy within 1.5–3 h after injection. Proper preparation of the radiotracer is important because the required size of the colloid, less than 100 nm, is critical to ensure fast drainage from the prostate gland, as has been shown for the proprietary product. We recommend that others who use our practice procedure work with their local radiopharmacy to obtain sulfur colloid that has been prefiltered with a 100-nm membrane filter.

A limitation of our study was that only patients with an intact and previously untreated prostate were included. We chose not to include postprostatectomy patients because of uncertainty as to the appropriate places to inject the radiotracer in this setting and the known altered drainage patterns after previous therapies (15). Another limitation of our study was the absence of definitive proof as to exactly how the information obtained through this lymphoscintigraphy technique may have altered our treatment fields. Such a detailed analysis is under way. On the basis of the work of

others, we do expect to find evidence supporting the routine use of sentinel node imaging (9,16).

Unlike common use of lymphoscintigraphy for surgical management of cancer, our prostate lymphoscintigraphy was to use SPECT/CT to provide tomographic information on lymphatic drainage through sentinel and secondary nodes, allowing radiation treatment for these patients to be planned using individualized irradiation fields. Clearly, in at least 2 cases the sentinel node images resulted in a substantial altering of the fields. In these 2 cases, the primary drainage included common iliac nodes above the level of L5–S1 (our standard superior border). In addition, in all cases we applied slightly wider margins and delivered a slightly higher dose to sentinel nodal areas. We also used tighter margins and consequently lower doses to nonsentinel nodal drainage areas. This strategy, at least in theory, should result in enhanced nodal control and reduced toxicity due to smaller irradiated volumes to uninvolved normal tissues, such as the small bowel.

Finally, another interesting methodologic approach that could enhance our practice procedure for SPECT/CT prostate lymphoscintigraphy is to use high-amperage CT, commonly applied in diagnostic multidetector CT scanners, instead of the low-amperage CT that was used in our studies, when combined with SPECT data. The high-amperage CT can reveal small lymph nodes in greater detail; thus, it will be easier to identify the anatomic locations of lymph nodes on SPECT images.

CONCLUSION

We successfully performed a 10-patient study to establish a SPECT/CT practice procedure for prostate lymphoscintigraphy, with a goal of using the information obtained for planning radiation treatment. The use of filtered ^{99m}Tc -sulfur nanocolloid seems appropriate for this indication, and the 1.5- to 3-h imaging window is favorable in clinical practice.

DISCLOSURE STATEMENT

The costs of publication of this article were defrayed in part by the payment of page charges. Therefore, and solely to indicate this fact, this article is hereby marked “advertisement” in accordance with 18 USC section 1734.

ACKNOWLEDGMENTS

We thank Marilyn Robinson at the University of California, San Francisco, for her help with coordinating the clinical study. We also thank Chang-Lae Lee, who helped with radiation dose calculations using biokinetic data. This study was partially funded by National Cancer

Institute grant K25 CA114254. No other potential conflict of interest relevant to this article was reported.

REFERENCES

1. Spiotto MT, Hancock SL, King CR. Radiotherapy after prostatectomy: improved biochemical relapse-free survival with whole pelvic compared with prostate bed only for high-risk patients. *Int J Radiat Oncol Biol Phys*. 2007;69:54–61.
2. Weckermann D, Dorn R, Trefz M, Wagner T, Wawroschek F, Harzmann R. Sentinel lymph node dissection for prostate cancer: experience with more than 1,000 patients. *J Urol*. 2007;177:916–920.
3. Touijer K, Rabbani F, Otero JR, et al. Standard versus limited pelvic lymph node dissection for prostate cancer in patients with a predicted probability of nodal metastasis greater than 1%. *J Urol*. 2007;178:120–124.
4. Briganti A, Karakiewicz PI, Chun FK, et al. Percentage of positive biopsy cores can improve the ability to predict lymph node invasion in patients undergoing radical prostatectomy and extended pelvic lymph node dissection. *Eur Urol*. 2007;51:1573–1581.
5. Briganti A, Gallina A, Suardi N, et al. A nomogram is more accurate than a regression tree in predicting lymph node invasion in prostate cancer. *BJU Int*. 2008;101:556–560.
6. Wagner M, Sokoloff M, Daneshmand S. The role of pelvic lymphadenectomy for prostate cancer: therapeutic? *J Urol*. 2008;179:408–413.
7. Roach M III, DeSilvio M, Valicenti R, et al. Whole-pelvis, “mini-pelvis,” or prostate-only external beam radiotherapy after neoadjuvant and concurrent hormonal therapy in patients treated in the Radiation Therapy Oncology Group 9413 trial. *Int J Radiat Oncol Biol Phys*. 2006;66:647–653.
8. Ploysongsang SS, Aron BS, Shehata WM. Radiation therapy in prostate cancer: whole pelvis with prostate boost or small field to prostate? *Urology*. 1992;40:18–26.
9. Ganswindt U, Paulsen F, Corvin S, et al. Optimized coverage of high-risk adjuvant lymph node areas in prostate cancer using a sentinel node-based, intensity-modulated radiation therapy technique. *Int J Radiat Oncol Biol Phys*. 2007;67:347–355.
10. Warncke SH, Mattei A, Fuechsel FG, Z’Brun S, Krause T, Studer UE. Detection rate and operating time required for gamma probe-guided sentinel lymph node resection after injection of technetium-99m nanocolloid into the prostate with and without preoperative imaging. *Eur Urol*. 2007;52:126–132.
11. Alicikus ZA, Yamada Y, Zhang Z. Ten-year outcomes of high-dose, intensity-modulated radiotherapy for localized prostate cancer. *Cancer*. 2011;117:1429–1437.
12. Ganswindt U, Paulsen F, Corvin S. Intensity modulated radiotherapy for high risk prostate cancer based on sentinel node SPECT imaging for target volume definition. *BMC Cancer*. 2005;5:91.
13. Jimenez IR, Roca M, Vega E, et al. Particle sizes of colloids to be used in sentinel lymph node radiolocalization. *Nucl Med Commun*. 2008;29:166–172.
14. Holl G, Dorn R, Wengenmair H, Weckermann D, Sciuk J. Validation of sentinel lymph node dissection in prostate cancer: experience in more than 2,000 patients. *Eur J Nucl Med Mol Imaging*. 2009;36:1377–1382.
15. Vermeeren L, Muller SH, Meinhardt W, Valdes Olmos RA. Optimizing the colloid particle concentration for improved preoperative and intraoperative image-guided detection of sentinel nodes in prostate cancer. *Eur J Nucl Med Mol Imaging*. 2010;37:1328–1334.
16. Ganswindt U, Schilling D, Müller AC, Bares R, Bartenstein P, Belka C. Distribution of prostate sentinel nodes: a SPECT-derived anatomic atlas. *Int J Radiat Oncol Biol Phys*. 2011;79:1364–1372.
17. Alazraki NP, Eshima D, Eshima LA, et al. Lymphoscintigraphy, the sentinel node concept, and the intraoperative gamma probe in melanoma, breast cancer, and other potential cancers. *Semin Nucl Med*. 1997;27:55–67.
18. Hung JC, Wiseman GA, Wahner HW, Mullan BP, Taggart TR, Dunn WL. Filtered technetium-99m-sulfur colloid evaluated for lymphoscintigraphy. *J Nucl Med*. 1995;36:1895–1901.
19. Stabin MG, Sparks RB, Crowe E. OLINDA/EXM: the second-generation personal computer software for internal dose assessment in nuclear medicine. *J Nucl Med*. 2005;46:1023–1027.
20. Wengenmair H, Kopp J, Vogt H, et al. Sentinel lymph node diagnosis in prostatic carcinoma: II. Biokinetics and dosimetry of ^{99m}Tc -nanocolloid after intraprostatic injection [in German]. *Nuklearmedizin*. 2002;41:102–107.